IMAGING OF MASS DISTRIBUTIONS FROM PARTIAL DOMAIN MEASUREMENT

M. HRIZI, A.A. NOVOTNY, AND M. HASSINE

Abstract. This paper deals with an inverse source problem governed by the Poisson equation. The aim is to reconstruct multiple anomalies from internal observation data within an arbitrary sub-region. The considered model problem is motivated by various applications such as the identification of geological anomalies underneath the Earth's surface. To overcome the ill-posedness, the inverse problem is formulated as a self-regularized topology optimization one. A *least-square* functional measuring the misfit between the observed quantities and the values provided by the model problem is introduced. The misfit function involves a regularization term penalizing the relative perimeter of the unknown domain. Finally, it is minimized with respect to a finite number of circular-shaped anomalies. The existence, uniqueness, and stability of the solution to the inverse problem are demonstrated. The reconstruction process is based on the topological derivative method. The variation of the shape functional with respect to a small geometric perturbation is studied and the leading terms of a second-order topological asymptotic expansion are derived. A non-iterative reconstruction algorithm is developed via the minimization of the obtained asymptotic formula with respect to the location and size parameters of the unknown set of anomalies. The efficiency and accuracy of the proposed approach are justified by some numerical experiments.

1. Introduction

In this paper, we analyze an inverse source problem governed by the two-dimensional Poisson equation. The aim is the reconstruction of a mass density distribution with support within a geometrical domain with the help of internal partial measurements of the potential field. This problem is motivated by various applications such as gravimetry, where the goal is to determine Earth's density distribution from the measurement of the gravity on the surface of the Earth [32].

The detection of mass distribution in a geometrical domain from total or partial boundary measurements has been the subject of several theoretical and numerical research works. In [6, 31] the authors established some theoretical results to reconstruct the unknown source from over-determined boundary measurements of the Poisson equation solutions. Isakov [32] proved an identifiability result for anomalies having star-shaped or convex in one direction supports. Then, El-Badia and Ha-Duong [21] established a uniqueness result for the problem of determining multiply-connected ball-shaped anomalies from a single Cauchy data. Hettlich and Rundell proposed in [28] a Newton-type iterative method for solving an anomaly shape reconstruction problem. In the same context, Hanke and Rundell [27] used the rational approximation method to solve inverse source problems for determining hidden obstacles. Based on the domain derivative, Martins [35] developed a decomposition method based on the Kirsch-Kress technique and a Newton-type algorithm for reconstructing a characteristic source functions in a potential problem, from the knowledge of full and partial boundary data. While Liu [34] proposed

Key words and phrases. Inverse source problem, partial domain measurement, topological derivative method, noniterative reconstruction algorithm.

an iterative approach based on the shape derivative. They applied the gradient descent algorithm (GDA) and trust-region-reflective procedure to reconstruct the location, size, and shape of the source.

In the context of gravimetry, Canelas *et al.* [14] solved this reconstruction problem in the two-dimensional case from complete boundary measurements. They proposed an approach based on the minimization of a Kohn-Vogelius type functional via a second-order topological sensitivity analysis. The same ideas has been exploited in [15] for recovering two and three spatial dimensions anomalies from incomplete (partial) boundary measurements. More recently, Menoret *et al.* [37] combined the Kohn-Vogelius formulation and a second-order topological gradient method for determining the support of a source-term, but without using the Newtonian potential to complement the unavailable information about the hidden boundary as presented in [15].

In most of the works mentioned above, the proposed geometric reconstruction approaches are developed with the help of boundary measurements. In the present paper, we address the problem of multiples anomalies reconstruction using local internal observation data. More precisely, we aim to reconstruct an unknown source-term support $\omega^\star \subset \Omega$ from a local interior measurement of the associated potential taken within an arbitrary sub-region $\Omega_0 \subset \Omega$, where $\Omega \subset \mathbb{R}^2$. In order to overcome the ill-posedness, the considered inverse problem is reformulated as a self-regularized topology optimization one where the mass distribution is the unknown variable. The considered misfit function contains two main terms. The first one is defined by a *least-square* functional, which measures the difference between the observed values and the fitted values provided by the model in the sub-region $\Omega_0 \subset \Omega$. The second one involves a regularization term penalizing the relative perimeter of the domains. To reconstruct the location, size, shape and number of the mass density distributions in the geometrical domain Ω, we propose an approach based on the second-order topological derivative method. The topological sensitivity analysis is used to estimate the variation of the *least-squares* functional with respect to a finite number of ball-shaped trial anomalies. The second-order topological gradient is exploited to develop an efficient and fast reconstruction algorithm. The main advantages of our numerical procedure are justified by some numerical investigations.

The rest of this paper is organized as follows. Section 2 states the inverse source problem and formulates it as a topology optimization one. In Section 3, we introduce some notations and we present some theoretical results concerning existence, uniqueness and stability of the considered optimization problem. Whereas, in Section 4 we derive the asymptotic expansion of a *least-square* functional with respect to a finite number of circular-shaped anomalies. The resulting Newton-type method is presented in Section 5, together with the associated reconstruction algorithm. In Section 6, we present numerical examples that demonstrate the effectiveness of the devised reconstruction algorithm. Finally, the paper ends with some concluding remarks in Section 7.

2. Problem formulation

Let $\Omega \subset \mathbb{R}^2$ be an open and bounded domain with Lipschitz boundary $\partial\Omega$. We consider the problem of determining a source term $f^\star$ in the following boundary value problem:

$$\left\{ \begin{array}{rcll} -\Delta z & = & f^\star & \text{in } \Omega, \\ z & = & 0 & \text{on } \partial\Omega, \end{array} \right. \tag{2.1}$$

from internal measurements of the potential z taken within an open sub-domain Ω_0 strictly included in Ω (i.e. $\Omega_0 \Subset \Omega$).

Based on the underlying physical motivations as mentioned in the introduction section, the source term to be reconstructed $f^\star$ is modeled here as a mass density distribution, namely,

$$f^\star = \chi_{\omega^\star}, \tag{2.2}$$

where $\chi_{\omega^\star}$ is the characteristic function of the unknown sub-domain $\omega^\star \subset \Omega \backslash \overline{\Omega_0}$.

In order to present the considered inverse source problem, we firstly introduce the set of the admissible solutions. It contains the characteristic functions having the form:

$$\mathcal{A}(\Omega) = \{\chi_\omega : \Omega \mapsto \mathbb{R} \mid \chi_\omega = 1 \text{ in } \omega \text{ and } \chi_\omega = 0 \text{ in } \Omega \setminus \omega, \text{ such that } P_\Omega(\omega) \leq C\}, \tag{2.3}$$

where $C > 0$ is a given constant, $\omega \subset \Omega \backslash \overline{\Omega_0}$ is a Lebesgue measurable set, and $P_\Omega(\omega)$ denotes the relative perimeter of ω in Ω, namely

$$P_\Omega(\omega) = \sup \Big\{ \int_\Omega \chi_\omega \, \mathrm{div}\varphi \;\Big|\; \varphi \in \mathcal{C}_c^1(\Omega)^2, \ \|\varphi\|_{L^\infty(\Omega)} \leq 1 \Big\},$$

with $\mathcal{C}_c^1(\Omega)$ is the space of continuously differentiable functions with compact support in Ω and $\|.\|_{L^\infty(\Omega)}$ is the essential supremum norm. Moreover, we use the notation $\int_\Omega u$ to the classical Lebesgue integral $\int_\Omega u(x)\mathrm{d}x$.

For each element χ_ω belongs to $\mathcal{A}(\Omega)$, we denote by u_ω the solution to the following boundary value problem

$$\left\{ \begin{array}{rcll} -\Delta u_\omega & = & \chi_\omega & \text{in } \Omega, \\ u_\omega & = & 0 & \text{on } \partial\Omega. \end{array} \right. \tag{2.4}$$

Assuming that the given measured data in Ω_0 is given by $z_{|_{\Omega_0}}$, where z is the potential related to the actual source term $f^\star = \chi_{\omega^\star}$, (i.e. z solves (2.1)). Thus, the inverse problem to be solved consists in finding $\chi_{\omega^\star} \in \mathcal{A}(\Omega)$ such that the associated potential u_ω approximate as most as possible the measured data in the sub-domain Ω_0.

According to this observation, the inverse reconstruction problem can be formulated as a topological optimization one. For this purpose, we consider a weaker formulation of the considered inverse problem which consists in solving the topology optimization problem of the form

$$\underset{\chi_\omega \in \mathcal{A}(\Omega)}{\text{Minimize}} \ \mathcal{J}(\chi_\omega, u_\omega), \tag{2.5}$$

where the cost function $\mathcal{J}$ is defined by

$$\mathcal{J}(\chi_\omega, u_\omega) := J(\chi_\omega) = \int_{\Omega_0} \Big(u_\omega - z\Big)^2 + \rho P_\Omega(\omega) \tag{2.6}$$

with $\rho > 0$ is a regularization parameter.

3. Analysis of the minimization problem

In this section, we discuss two theoretical questions related to the considered inverse problem. The first one is devoted to the existence of an optimal solution. The second one is concerned with the stability notion. We start our analysis by introducing some definitions as well as some useful results.

3.1. Notations and preliminary results.

Let $L^q(\Omega)$ and $H^p(\Omega)$ be the usual Lebesgue and Sobolev spaces. In a Banach space $\mathcal{Y}$, we denote the weak convergence of a sequence $\{\mathcal{T}_n\}_n$ to $\mathcal{T}$ by

$$\mathcal{T}_n \rightharpoonup \mathcal{T} \text{ in } \mathcal{Y} \text{ as } n \to \infty.$$

Now, we briefly introduce the space of functions with bounded total variation. For more details the reader may refer to [9]. A function u belonging to $L^1(\Omega)$ is said to be of bounded total variation if

$$|Du|(\Omega) := \sup\Big\{ \int_\Omega u \text{ div } \varphi \;\Big|\; \varphi \in \mathcal{C}_c^1(\Omega)^2,\ \|\varphi\|_{L^\infty(\Omega)} \leq 1\Big\}.$$

Let $BV(\Omega)$ be the space of functions of bounded total variation (BV-functions). It can then be defined as

$$BV(\Omega) = \Big\{u \in L^1(\Omega) \;\Big|\; |Du|(\Omega) < \infty\Big\}$$

and equipped with the natural norm

$$\|u\|_{BV(\Omega)} = \|u\|_{L^1(\Omega)} + |Du|(\Omega).$$

Finally, we recall the following preliminary results, which will be used in the sequel. For more details and proofs one can consult [20, Theorem 6.3 in Chapter 5].

Lemma 1. *Let $\{\mathcal{O}_n\}_n$ be a sequence of measurable domains in Ω for which there exists a constant $c > 0$ such that*

$$P_\Omega(\mathcal{O}_n) \leq c, \quad \forall\, n.$$

Then, there exist a measurable set $\mathcal{O}^*$ in Ω and a subsequence $\{\mathcal{O}_{n_k}\}_k$ such that

$$\chi_{\mathcal{O}_{n_k}} \to \chi_{\mathcal{O}^*} \text{ in } L^1(\Omega) \text{ as } k \to \infty \tag{3.1}$$

and

$$P_\Omega(\mathcal{O}^*) \leq \liminf_{k\to\infty} P_\Omega(\mathcal{O}_{n_k}) \leq c. \tag{3.2}$$

Remark 2. *When $P_\Omega(\omega) < \infty$, we say that ω has finite perimeter in Ω. In this case the relative perimeter $P_\Omega(\omega)$ of ω coincides with the total variation of the distributional gradient of the characteristic function of ω :*

$$P_\Omega(\omega) = |D\chi_\omega|(\Omega).$$

The penalization of the error function ($L^2(\Omega_0)$-norm) by the relative perimeter P_Ω is relevant for the existence of optimal solution of the optimization problem (2.5), which will be discussed in the next section.

3.2. **Existence and uniqueness of a minimizer.** This section is concerned with the existence of an optimal solution to the considered problem (2.5). The obtained result is summarized in the following theorem.

Theorem 3. *The minimization problem* (2.5) *admits at least one solution.*

Proof. Since the function J from (2.6) is bounded from below by zero, there exists a minimizing sequence $\{\chi_{\omega_n}\}_n \subset \mathcal{A}(\Omega)$ such that

$$\lim_{n\to\infty} J(\chi_{\omega_n}) = \inf_{\chi_\omega \in \mathcal{A}(\Omega)} J(\chi_\omega).$$

By the definition of the admissible solutions, we deduce that $\{\omega_n\}_n$ is a sequence of measurable domains in Ω such that $P_\Omega(\omega_n) \leq C$. Therefore, in view of Lemma 1, there exist a measurable set $\omega^\star \in \Omega$ and a subsequence of $\{\chi_{\omega_n}\}_n$, still denoted by $\{\chi_{\omega_n}\}_n$, such that

$$\chi_{\omega_n} \to \chi_{\omega^\star} \text{ in } L^1(\Omega) \text{ as } n \to \infty$$

and

$$P_\Omega(\omega^\star) \leq \liminf_{n\to\infty} P_\Omega(\omega_n) \leq C.$$

Consequently,

$$\chi_{\omega^\star} \in \mathcal{A}(\Omega).$$

Now, we shall prove that $\chi_{\omega^\star}$ is indeed the unique minimizer to (2.5). For each $n \in \mathbb{N}$, let us consider u_{ω_n} the solution of the following boundary value problem

$$\left\{ \begin{array}{rcll} -\Delta u_{\omega_n} & = & \chi_{\omega_n} & \text{in } \Omega, \\ u_{\omega_n} & = & 0 & \text{on } \partial\Omega. \end{array} \right. \tag{3.3}$$

By taking u_{ω_n} as test function in the weak formulation of (3.3), one can deduce

$$\|u_{\omega_n}\|_{H_0^1(\Omega)} \leq c, \tag{3.4}$$

where c is a positive constant depending only on Ω. Thus, the sequence $\{u_{\omega_n}\}_n$ is bounded in $H_0^1(\Omega)$. This indicates the existence of some $u^\star \in H_0^1(\Omega)$ and a sub-sequence of $\{u_{\omega_n}\}_n$, again still denoted by $\{u_{\omega_n}\}_n$, such that

$$u_{\omega_n} \rightharpoonup u^\star \text{ in } H_0^1(\Omega) \text{ as } n \to \infty. \tag{3.5}$$

We claim

$$u^\star = u_{\omega^\star}.$$

In other hand, the variational formulation of (3.3) implies

$$\int_\Omega \nabla u_{\omega_n} \cdot \nabla w = \int_\Omega \chi_{\omega_n} w, \ \ \forall w \in H_0^1(\Omega). \tag{3.6}$$

Due to (3.5), it follows

$$\nabla u_{\omega_n} \rightharpoonup \nabla u^\star \text{ in } L^2(\Omega) \times L^2(\Omega) \text{ as } n \to \infty.$$

Tending n to infinity, from (3.6) one can obtain

$$\int_\Omega \nabla u^\star \cdot \nabla w = \int_\Omega \chi_{\omega^\star} w, \ \ \forall w \in H_0^1(\Omega). \tag{3.7}$$

Thanks to the uniqueness of the limit, one can conclude that

$$u^\star = u_{\omega^\star}.$$

The last part of this proof is due to the lower semi-continuity of the function J. Indeed, it is well known that the $L^2(\Omega_0)$-norm is lower semi-continuous. The lower semi-continuity of the second term in J (the perimeter function) from Lemma 1 (see aslo [7, Proposition 10.1.1]). Then, exploiting the lower semi-continuity of J and the above convergence results, one can derive

$$\begin{aligned} J(\chi_{\omega^\star}) &= \int_{\Omega_0} \Big(u^\star - z\Big)^2 + \rho P_\Omega(\omega^\star) \\ &\leq \liminf_{n\to\infty} \int_{\Omega_0} \Big(u_{\omega_n} - z\Big)^2 + \rho \liminf_{n\to\infty} P_\Omega(\omega_n) \\ &\leq \liminf_{n\to\infty} J(\chi_{\omega_n}) = \inf_{\chi_\omega \in \mathcal{A}(\Omega)} J(\chi_\omega), \end{aligned}$$

indicating that χ_{ω^*} is indeed a minimizer to the optimization problem (2.5). Furthermore, the convexity of $J(\chi_\omega)$ follows from the convexity of the error function (L^2-norm) and the penalty term [19], which implies the uniqueness of χ_{ω^*}. □

3.3. **Stability result.** In this section, we will discuss the stability question related to the minimization problem (2.5). Let $\{z_n\}_n$ be a sequence of measurements of the potential in Ω_0. For each $n \in \mathbb{N}$, we denote by χ_{ω_n} the solution to the following minimization problem

$$\underset{\chi_\omega \in \mathcal{A}(\Omega)}{\text{Minimize}}\, J_n(\chi_\omega),$$

with J_n is the cost function defined by

$$J_n(\chi_\omega) := \int_{\Omega_0} \Big(u_\omega - z_n\Big)^2 + \rho P_\Omega(\omega).$$

In the following theorem, we examine the convergence of the sequence $\{\chi_{\omega_n}\}_n$ when the measured data z_n tends to z in L^2 as $n \to +\infty$.

Theorem 4. *If z_n tends to z in $L^2(\Omega_0)$ as $n \to +\infty$. Then, the sequence $\{\chi_{\omega_n}\}_n$ converges strongly in $L^1(\Omega)$ to the minimizer of the optimization problem* (2.5).

Proof. The unique existence of each χ_{ω_n} is guaranteed by Theorem 3. Since $P_\Omega(\omega_n) \leq C$, thus from Lemma 1, there exists $\chi_{\omega^\star} \in \mathcal{A}(\Omega)$ and a subsequence of $\{\chi_{\omega_n}\}_n$, still denoted by $\{\chi_{\omega_n}\}_n$, such that

$$\chi_{\omega_n} \to \chi_{\omega^\star} \text{ in } L^1(\Omega) \text{ as } n \to \infty.$$

Now it suffices to show that $\chi_{\omega^\star}$ is indeed the unique solution to the minimization problem (2.5). Actually, after repeating the same argument as that in the proof of Theorem 3, one can derive

$$u_{\omega_n} \rightharpoonup u_{\omega^\star} \text{ in } H_0^1(\Omega) \text{ as } n \to \infty, \tag{3.8}$$

up to taking a further sub-sequence. Using the convergence of z_n to z when $n \to +\infty$ and from (3.8), one can obtain

$$u_{\omega_n} - z_n \rightharpoonup u_{\omega^\star} - z \text{ in } L^2(\Omega_0) \text{ as } n \to \infty.$$

Consequently, for any $\chi_\omega \in \mathcal{A}(\Omega)$, again we take advantage of the the lower semi-continuity of the L^2-norm and the lower semi-continuity of the perimeter to deduce

$$\begin{aligned}
J(\chi_{\omega^\star}) &= \int_{\Omega_0} \Big(u_{\omega^\star} - z\Big)^2 + \rho P_\Omega(\omega^\star) \\
&\leq \liminf_{n\to\infty} \int_{\Omega_0} \Big(u_{\omega_n} - z_n\Big)^2 + \rho \liminf_{n\to\infty} P_\Omega(\omega_n) \\
&\leq \liminf_{n\to\infty} \Big[\int_{\Omega_0} \Big(u_{\omega_n} - z_n\Big)^2 + \rho P_\Omega(\omega_n)\Big] \\
&\leq \lim_{n\to\infty} \Big[\int_{\Omega_0} \Big(u_{\omega} - z_n\Big)^2 + \rho P_\Omega(\omega)\Big].
\end{aligned}$$

Then, it follows

$$J(\chi_{\omega^\star}) \leq \int_{\Omega_0} \Big(u_\omega - z\Big)^2 + \rho P_\Omega(\omega) = J(\chi_\omega), \quad \forall \chi_\omega \in \mathcal{A}(\Omega),$$

which implies that $\chi_{\omega^\star}$ is a solution to the minimization problem (2.5). □

4. Sensitivity analysis

The considered inverse problem (2.1) has been rewritten in the form of a topology optimization problem (2.5), which will be solved with the help of a fast and accurate approach based on the topological derivative method [38, 39]. The topological derivative was introduced in the field of shape optimization in [22, 43] and was for the first time mathematically justified in [26, 44]. Since then, topological based gradient algorithms have been successfully applied for solving a wide range of relevant problems, such as cracks detection [4], images restoration and classification [8, 11], images segmentation [30], detection of small cavities in Stokes flow [1], localization of obstacles [17, 18], topology optimization of structures [5, 26], elastodynamic and acoustic inverse scattering [12, 42], fracture mechanics [3, 46], damage evolution phenomena [2, 47], and many other applications [40].

In the context of inverse problems, such numerical algorithms are non-iterative, free of initial guess and require only a minimal number of user defined algorithmic parameters, contrary to the traditional optimization procedure where many parameters must be adequately chosen (such as the initial guess, step size, regularization coefficient, ... etc) to enhance the stability of the numerical procedure and ensure the optimization process. Numerical simulations in the literature have shown that topological gradient based algorithms enjoy high robustness with respect to noisy input data. Hence, despite the large number of investigations concerning the topological sensitivity analysis method, the theoretical aspect of the robustness issue has not been addressed so far.

To solve the topology optimization problem (2.5), we propose in this work a fast and accurate detection approach based on both first and second topological gradients. To this end, we derive a second-order topological asymptotic expansion for the considered shape function $\mathcal{J}$ with respect to the presence of a finite number of ball-shaped anomalies. But before, let us introduce some notations and useful assumptions. Let $N \geq 1$ be a given integer. For each $1 \leq i \leq N$, we denote by $\mathcal{B}_{\varepsilon_i}(\hat{x}_i)$ the ball of radius ε_i and center $\hat{x}_i \in \Omega$. We assume that the balls $\mathcal{B}_{\varepsilon_i}(\hat{x}_i)$ are disjoints and strictly included inside the domain $\Omega \backslash \overline{\Omega_0}$; i.e.

$$\mathcal{B}_{\varepsilon_i}(\hat{x}_i) \cap \mathcal{B}_{\varepsilon_j}(\hat{x}_j) = \varnothing, \, \forall i, j \in \{1, ..., N\} \text{ and } i \neq j$$

$$\overline{\mathcal{B}_{\varepsilon_i}(\hat{x}_i)} \subset \Omega \text{ and } \overline{\mathcal{B}_{\varepsilon_i}(\hat{x}_i)} \cap \Omega_0 = \varnothing, \, \forall i = 1, ..., N.$$

From these elements, the perturbed counterpart of the characteristic source term χ_ω can be defined

$$\chi_{\omega_\varepsilon} = \chi_\omega + \sum_{i=1}^{N} \chi_{\mathcal{B}_{\varepsilon_i}(\hat{x}_i)}. \tag{4.1}$$

As mentioned above, the first-order topological derivative method provide a fast and accurate numerical optimization algorithm which means that no any additional regularization term is needed to stabilize the reconstruction process. Later on, this result was generalized to the second-order topological derivative by Novotny et al. [15, 16, 24, 25, 41]. More recently, in the context of gravimetry, Menoret et al. [37] discussed the robustness of the second-order topological gradient method of four different error norms. More precisely, they proved that the L^2-norms are more robust with respect to noise (numerically). However, this feature still needs to be mathematically proven. Hence, for the sake of simplicity, we neglect the influence of the regularization term in (2.6) by assigning a small value to the parameter ρ. Indeed, one can choose $\rho = |\varepsilon|^5$ where $\varepsilon = (\varepsilon_1, \cdots, \varepsilon_N)$ and $|\varepsilon| = \varepsilon_1 + ... + \varepsilon_N$. Then, $\rho P_\Omega(\omega) = o(|\varepsilon|^4)$ since $P_\Omega(\omega) \leq C$. Therefore, the cost functional

associated with the topologically perturbed domain can be evaluated as

$$\mathcal{J}(\chi_{\omega_\varepsilon}, u_\varepsilon) = \int_{\Omega_0} \Big(u_\varepsilon - z\Big)^2 + o(|\varepsilon|^4), \tag{4.2}$$

with u_ε be the solution of the perturbed boundary value problem

$$\left\{ \begin{array}{rcll} -\Delta u_\varepsilon &=& \chi_{\omega_\varepsilon} & \text{in} \quad \Omega, \\ u_\varepsilon &=& 0 & \text{on} \quad \partial\Omega. \end{array} \right. \tag{4.3}$$

Now, we are ready to establish an asymptotic formula describing the variation of $\mathcal{J}(\chi_{\omega_\varepsilon}, u_\varepsilon) - \mathcal{J}(\chi_\omega, u_\omega)$ with respect to ε. Firstly, let us introduce the following ansatz for the solution to the perturbed problem (4.3):

$$u_\varepsilon(x) = u_\omega(x) + \sum_{i=1}^{N} \pi\varepsilon_i^2 v_{\varepsilon_i}(x), \tag{4.4}$$

where v_{ε_i} is the solution of the following auxiliary boundary value problem for $i = 1, ..., N$: Find v_{ε_i}, such that :

$$\left\{ \begin{array}{rcll} -\Delta v_{\varepsilon_i} &=& \frac{1}{\pi\varepsilon_i^2}\chi_{\mathcal{B}_{\varepsilon_i}(\hat{x}_i)} & \text{in} \quad \Omega, \\ v_{\varepsilon_i} &=& 0 & \text{on} \quad \partial\Omega. \end{array} \right. \tag{4.5}$$

Since each v_{ε_i} depends on ε_i in the ball $\mathcal{B}_{\varepsilon_i}(\hat{x}_i)$, we can decompose it into two parts, namely

$$v_{\varepsilon_i}(x) = p_{\varepsilon_i}(x) + q_i(x), \tag{4.6}$$

where p_{ε_i} is solution of the following boundary value problem defined in a big ball $\mathcal{B}_R(\hat{x}_i) \supset \Omega$ of radius R and centered at $\hat{x}_i$: Find p_{ε_i}, such that

$$\left\{ \begin{array}{rcll} -\Delta p_{\varepsilon_i} &=& \frac{1}{\pi\varepsilon_i^2}\chi_{\mathcal{B}_{\varepsilon_i}(\hat{x}_i)} & \text{in} \quad \mathcal{B}_R(\hat{x}_i), \\ p_{\varepsilon_i} &=& \frac{1}{2\pi}\ln R & \text{on} \quad \partial\mathcal{B}_R(\hat{x}_i). \end{array} \right. \tag{4.7}$$

The above boundary value problem admits an explicit solution given by

$$p_{\varepsilon_i}(x) = \begin{cases} -\frac{1}{4\pi}\left(\frac{\|x-\hat{x}_i\|^2}{\varepsilon_i^2} + 2\ln\varepsilon_i - 1\right) & x \in \mathcal{B}_{\varepsilon_i}(\hat{x}_i), \\ -\frac{1}{2\pi}\ln\|x-\hat{x}_i\| & x \in \mathcal{B}_R(\hat{x}_i) \setminus \mathcal{B}_{\varepsilon_i}(\hat{x}_i). \end{cases} \tag{4.8}$$

In addition, q_i is the solution to the homogeneous canonical boundary value of the form problem

$$\left\{ \begin{array}{rcll} -\Delta q_i &=& 0 & \text{in} \quad \Omega, \\ q_i &=& \frac{1}{2\pi}\ln\|x-\hat{x}_i\| & \text{on} \quad \partial\Omega. \end{array} \right. \tag{4.9}$$

Therefore, the difference between u_ε and z can be obtained simply as

$$u_\varepsilon - z = u_\omega - z + \sum_{i=1}^{N} \pi\varepsilon_i^2 v_{\varepsilon_i}. \tag{4.10}$$

Since $\mathcal{B}_{\epsilon_i}(\hat{x}_i) \cap \Omega_0 = \varnothing$, then

$$v_{\varepsilon_i}(x) = p_i(x) + q_i(x), \quad \forall x \in \Omega_0, \tag{4.11}$$

with

$$p_i(x) := p_{\varepsilon_i}(x) = -\frac{1}{2\pi}\ln\|x-\hat{x}_i\|, \quad \forall x \in \Omega_0. \tag{4.12}$$

Consequently, after replacing (4.10) into (4.2), we can collect the terms in power of ε_i to get the following asymptotic expansion:

$$\mathcal{J}(\chi_{\omega_\varepsilon}, u_\varepsilon) - \mathcal{J}(\chi_\omega, u_\omega) = 2\sum_{i=1}^{N} \pi\varepsilon_i^2 \int_{\Omega_0} (u_\omega - z)h_i + \sum_{i,j=1}^{N} \pi\varepsilon_i^2 \pi\varepsilon_j^2 \int_{\Omega_0} h_i h_j + o(|\varepsilon|^4), \quad (4.13)$$

where we have considered (4.11) and introduced the notation $h_i = p_i + q_i$.

5. Reconstruction algorithm

In this section, we want to find a better approximation to the target $\omega^\star$ than the initial guess ω based on the topological asymptotic expansion of the shape functional (4.13). In particular, after disregarding the higher order terms of $o(|\varepsilon|^4)$, the following quantity can be introduced

$$\Psi(\alpha, \xi) = \alpha \cdot d(\xi) + \frac{1}{2} H(\xi)\alpha \cdot \alpha, \quad (5.1)$$

where vectors $\xi = (\hat{x}_1, \cdots, \hat{x}_N)$ and $\alpha = (\alpha_1, \cdots \alpha_N)$, with $\alpha_i = \pi\varepsilon_i^2$. The vector d and matrix H have entries

$$d(\xi) = \begin{pmatrix} d_1 \\ d_2 \\ \vdots \\ d_N \end{pmatrix} \quad \text{and} \quad H(\xi) = \begin{pmatrix} H_{11} & H_{12} & \cdots & H_{1N} \\ H_{21} & H_{22} & \cdots & H_{2N} \\ \vdots & \vdots & \ddots & \vdots \\ H_{N1} & H_{N2} & \cdots & H_{NN} \end{pmatrix}, \quad (5.2)$$

where

$$d_i = 2\int_{\Omega_0} (u_\omega - z)h_i \quad \text{and} \quad H_{ij} = 2\int_{\Omega_0} h_i h_j. \quad (5.3)$$

Given the general function of form (5.1), its minimum is trivially found when:

$$\langle D_\alpha \Psi(\alpha, \xi), \beta \rangle = 0, \quad \forall \beta \in \mathbb{R}^N. \quad (5.4)$$

Furthermore, given H_{ij} is symmetric positive definite, the minimum of the function $\Psi(\alpha, \xi)$ with respect to α is the global minimum. In particular,

$$(H(\xi)\alpha + d(\xi)) \cdot \beta = 0, \quad \forall \beta \in \mathbb{R}^N \quad \Rightarrow \quad H(\xi)\alpha = -d(\xi) \quad (5.5)$$

provided that $H = H^\top$. Therefore,

$$\alpha = \alpha(\xi) = -H(\xi)^{-1} d(\xi), \quad (5.6)$$

such that the quantity α, solving (5.6), becomes a function of the locations ξ. After replacing the solution of (5.6) into $\Psi(\alpha, \xi)$, defined by (5.1), the optimal locations ξ^* can be obtained from a combinatorial search over the domain Ω. These locations are the solutions to the following minimization problem:

$$\xi^* = \underset{\xi \in X}{\operatorname{argmin}} \left\{ \Psi(\alpha(\xi), \xi) = \frac{1}{2}\alpha(\xi) \cdot d(\xi) \right\}, \quad (5.7)$$

where X is the set of admissible locations of anomalies. Then, the optimal sources are characterized by the pair ξ^* and $\alpha^* = \alpha(\xi^*)$ of locations and sizes, respectively.

To summarize, we have introduced a second order topology optimization algorithm which is able to find the optimal sizes α^* of the hidden anomalies and their locations ξ^* for a given number N of trial balls. The inputs to the algorithm are:

- the vector d and the matrix H;
- the $M = \text{card}(X)$ points at which the system (5.6) is solved;

Algorithm 1: Second Order Reconstruction Algorithm

input : M, N;
output: the optimal solution α^*, ξ^*;

Initialization: $\Psi^* \leftarrow \infty$; $\alpha^* \leftarrow 0$; $\xi^* \leftarrow 0$;
for $i_1 \leftarrow 1$ **to** M **do**
  for $i_2 \leftarrow i_1 + 1$ **to** M **do**
    $\vdots$
    for $i_N \leftarrow i_{N-1} + 1$ **to** M **do**
      $$d \leftarrow \begin{bmatrix} d_{(i_1)} \\ d_{(i_2)} \\ \vdots \\ d_{(i_N)} \end{bmatrix}; \quad H \leftarrow \begin{bmatrix} H_{(i_1,i_1)} & H_{(i_1,i_2)} & \cdots & H_{(i_1,i_N)} \\ H_{(i_2,i_1)} & H_{(i_2,i_2)} & \cdots & H_{(i_2,i_N)} \\ \vdots & \vdots & \ddots & \vdots \\ H_{(i_N,i_1)} & H_{(i_N,i_2)} & \cdots & H_{(i_N,i_N)} \end{bmatrix};$$
      $\mathcal{I} \leftarrow (i_1, i_2, \ldots, i_N)$; $\xi \leftarrow \Pi(\mathcal{I})$; $\alpha \leftarrow -H^{-1}d$; $\Psi \leftarrow \frac{1}{2} d \cdot \alpha$;
      if $\Psi < \Psi^*$ **then**
        $\xi^* \leftarrow \xi$; $\alpha^* \leftarrow \alpha$; $\Psi^* \leftarrow \Psi$;
      end if
    end for
  end for
end for
return α^*, ξ^*;

- the number N of anomalies to be reconstructed.

The algorithm returns the optimal sizes α^* and locations ξ^*. For the reader convenience, the above procedure is written in pseudo-code format as shown in Algorithm 1. In the algorithm, Π maps the vector of nodal indices $\mathcal{I} = (i_1, i_2, \ldots, i_N)$ to the corresponding vector of nodal coordinates ξ. For further applications of this algorithm, we refer to [15, 23, 25].

In Algorithm 1, optimal source locations ξ^* are obtained through a combinatorial search over M trial points sampling the set of admissible locations X. As a result, the computational complexity $\mathcal{C}(M, N)$ of the algorithm can be evaluated by the formula

$$\mathcal{C}(M, N) \approx \left(\begin{array}{c} M \\ N \end{array} \right) N^3 = \frac{M!}{N!(M-N)!} N^3.$$

In Figure 1, the graphs of $N \times \log_{10}(\mathcal{C}(M, N))$ for $M = 100$ and $M = 400$ are plotted as solid and dashed lines, respectively. As can be seen from the display, the computational cost of the algorithm may become prohibitive for $N \approx M/2$. Note that for $N = M$ there is no combinatorial search to perform and thus the complexity of the algorithm is of $O(N^3)$. This feature has been successfully explored in the design of electromagnetic antennas in hyperthermia therapy [36].

Finally, let us point out some interesting features of the Algorithm 1: (a) when the number $N^\star$ of target anomalies is unknown, the algorithm can be started based on the assumption that there exists $N > N^\star$ anomalies and then we should find a number $(N - N^\star)$ of trial balls with negligible sizes; (b) if the center of the target anomaly $\xi^\star$ does not belong to the set of admissible locations X, the algorithm returns a location ξ^* which is the closest to the true one $\xi^\star$; and (c) since a combinatorial search over all the M-points

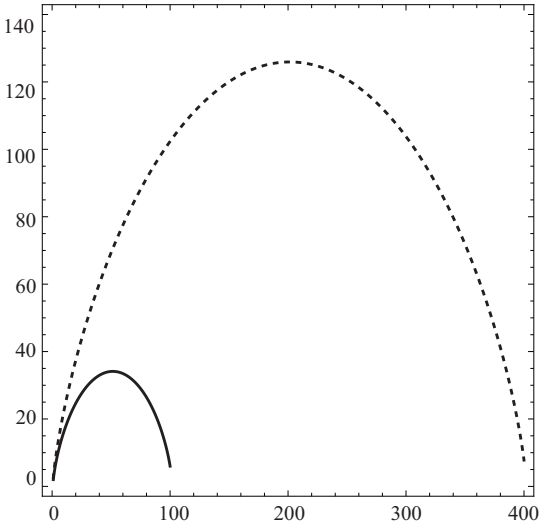

FIGURE 1. Complexity order of Algorithm 1: $N \times \log_{10}(\mathcal{C}(M,N))$ for $M = 100$ (solid) and $M = 400$ (dashed).

of the set X has to be performed, this exhaustive search becomes rapidly infeasible for $M \approx 2N$, as N increases. In the ensuing numerical examples, we set $N \ll M$, with N small, so that Algorithm 1 runs in a few seconds for all examples.

6. Numerical results

Let us consider a domain $\Omega = (0,1) \times (0,1)$, which is discretized with three-node finite elements. The mesh is generated from a grid of size 160×160, where each resulting square is divided into four triangles, leading to 102.400 elements. The set of admissible locations X is obtained by selecting 181 uniformly distributed interior nodes from the finite elements mesh. In order to verify the robustness of the method with respect to noisy data, the true source term $f^\star$ is corrupted with White Gaussian Noise (WGN). In particular, the target source $f^\star$ is replaced by

$$f^\star_\sigma(x) = f^\star(x) + \sigma\tau(x), \tag{6.1}$$

where $\tau : \Omega \mapsto \mathbb{R}$ is a normal random variable of zero mean and σ corresponds to the noise level. Note that in this context, noisy data can be interpreted as modeling uncertainties. In addition, to quantify the impact of the noisy data in the associated potential, the following definition for the effective noise level is introduced

$$\mathcal{E} = \frac{\|z - z_\sigma\|_{L^2(\Omega_0)}}{\|z\|_{L^2(\Omega_0)}} \times 100\ [\%], \tag{6.2}$$

where z and z_σ are the potentials obtained from the original $f^\star$ and corrupted sources $f^\star_\sigma$, respectively. Finally, we set $\omega = \varnothing$, which means that all the examples are free of initial guess.

6.1. **Example 1.** In this example we consider the reconstruction of two anomalies, one L-shaped and another one circular. The experiment is free of noise, namely $\sigma = 0\%$. Figure 2(a) shows the target to be reconstructed in black together with the observable domain Ω_0 in grey, given by four quarter of circles of radius $\rho_0 = 0.01$ each one. By setting $N = 4$ trial balls, the obtained result is shown in Figure 2(b). Note that the

target can be properly approximated by a number of balls, even for a small amount of available information, in the case $|\Omega_0|/|\Omega| = \pi \times 10^{-4}$.

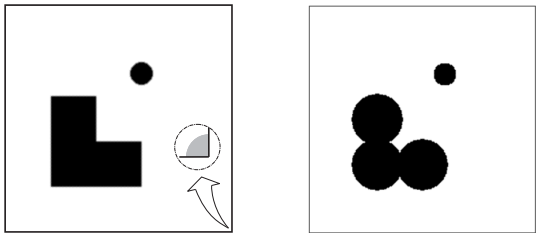

(a) Target (b) Result

FIGURE 2. Example 1: Target to be reconstructed in black and observable domain in gray (a), and obtained result for $N = 4$ trial balls (b).

6.2. **Example 2.** In this example we consider the reconstruction of a cross-shaped anomaly, as shown in Figure 3(a). The target is corrupted with $\sigma = 80\%$ of noise, according to Figure 3(b). The observable domain Ω_0 is given by four quarter of circles of radius ρ_0 each one, as in the previous example. However, in order to verify how sensitive is the reconstruction with respect to Ω_0, we consider different values for the radius ρ_0. The obtained results by setting $N = 1$ trial ball are presented in Figure 4 for ρ_0 equal to 0.02, 0.04, 0.10 and 0.20, with $\sigma = 80\%$ of noise. From an analysis of these figures, in the presence of noise, we observe that the less information is available, the worst is the result. Note that for $\rho_0 = 0.2$, the center of the trial ball coincides with the barycenter of the cross-shaped anomaly and the resulting volumes are very close to each other, even for such a high level of noise. In fact, let us introduce the quantity $\mu_\xi := \|\xi^* - \xi^\star\|$ measuring the distance between the barycenter $\xi^\star$ of the true cross-shaped anomaly of Figure 3(a) and the found center ξ^* of the trial ball. The convergence of the distance function μ_ξ with respect to the size ρ_0 of the observable domain Ω_0 is shown in Table 1, which confirms what it is observed in Figure 4. For the reader convenience, the effective noise levels $\mathcal{E}$ from (6.2), associated with each value of ρ_0 and $\sigma = 80\%$, are also reported in Table 1.

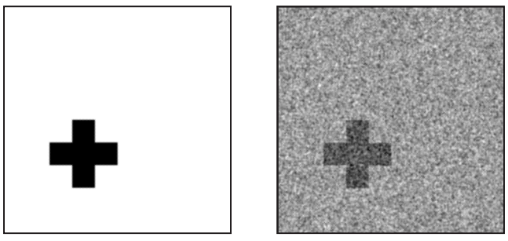

(a) Target (b) Source $f_\sigma^\star$

FIGURE 3. Example 2: Target to be reconstructed (a) and noisy source term $f_\sigma^\star$ for $\sigma = 80\%$ (b).

6.3. **Example 3.** In this example we consider the reconstruction of three ball-shaped anomalies of varying sizes. Figure 5 shows the target to be reconstructed in black together with the observable domain Ω_0 in grey, given by four quarter of circles of radius ρ_0 as in the previous examples, but with fixed $\rho_0 = 0.2$. The target is corrupted with varying levels of noise σ. The obtained results by setting $N = 3$ trial balls are presented in Figure

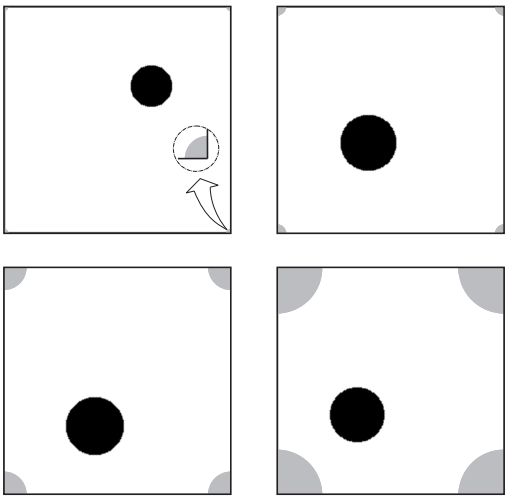

FIGURE 4. Example 2: Obtained reconstructions in black for varying observable domains Ω_0 in grey, with radius ρ_0 equal to 0.02, 0.04, 0.10 and 0.20, respectively, $N = 1$ trial ball and $\sigma = 80\%$ of noise.

TABLE 1. Example 2: Convergence of the distance function μ_ξ with respect to the size ρ_0 of the observable domain Ω_0 and effective noise levels $\mathcal{E}$.

ρ_0	0.02	0.04	0.10	0.20
μ_ξ	0.4243	0.0707	0.0707	0.0000
$\mathcal{E}$	11.36%	25.35%	41.50%	80.04%

6 for σ equal to 0%, 10%, 20% and 40% of noise. From an analysis of these figures, we observe that up to $\sigma = 20\%$, the reconstruction can be considered acceptable. For $\sigma = 40\%$ the solution starts to degrade. Finally, the effective noise levels $\mathcal{E}$ from (6.2) are reported in Table 2.

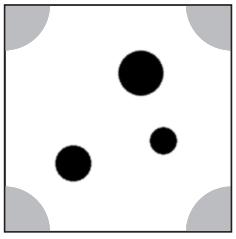

FIGURE 5. Example 3: Target to be reconstructed in black and observable domain in gray.

TABLE 2. Example 3: Effective noise levels $\mathcal{E}$ in [%].

σ	10	20	40
$\mathcal{E}$	1.31	2.62	5.23

Before present the last example, let us show two more results based on the same target to be reconstructed. In the first case, we consider the observable domain Ω_0 as shown in

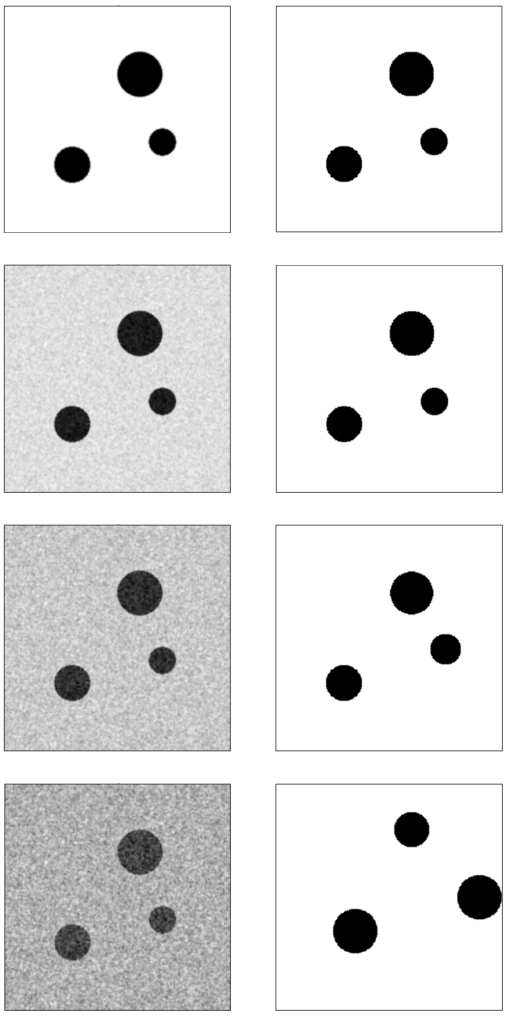

FIGURE 6. Example 3: Noisy source term $f_\sigma^\star$ (left) and reconstructions obtained from $N = 3$ trial balls (right), with 0%, 10%, 20% and 40% of noise, respectively.

Figure 7(a). By setting $N = 4$ trial balls in Algorithm 1, we obtain the result presented in Figure 7(b), where a tinny fourth ball pointed by the red arrow has been found, as expected. Finally, let us consider the case in which $\omega^\star \subset \Omega_0$ as shown in Figure 8(a), violating the assumption that the target domain $\omega^\star$ does not touch the observable domain Ω_0. The obtained result is presented in Figure 8(b), whose reconstruction is unexpected good since expansion (4.13) does not account for $\omega^\star \subset \Omega_0$. Actually, in this case the asymptotic analysis becomes more involved and some intermediate term between ε_i^2 and ε_i^4 of the form $\varepsilon_i^4 \ln(\varepsilon_i)$ would appear in the expansion (4.13).

6.4. **Example 4.** In this last example we consider the reconstruction of one ball-shaped anomaly. The observable domain Ω_0 is given by four quarter of circles of radius ρ_0 each one as in the previous examples, with $\rho_0 = 0.1$. The set of admissible locations X is obtained by selecting 21, 113, 481 and 1985 uniformly distributed interior nodes from the finite elements mesh. The true location $\xi^\star$ does not belongs to the first three set of admissible locations, but it belongs to the last one. The distance function $\mu_\xi = \|\xi^* - \xi^\star\|$ is considered, where $\xi^\star$ is the center of the true anomaly and ξ^* is the center of the trial

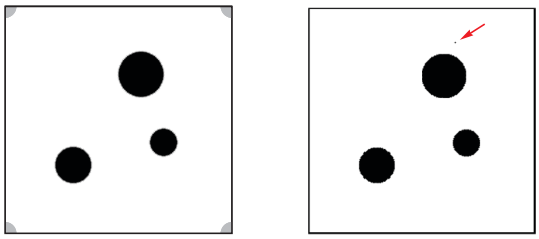

(a) Target (b) Result

FIGURE 7. Example 3: Target to be reconstructed in black and observable domain in gray (a), and obtained result for $N = 4$ trial balls (b). The red arrow is pointing to the fourth tinny ball.

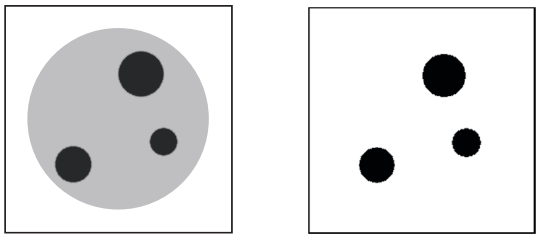

(a) Target (b) Result

FIGURE 8. Example 3: Target to be reconstructed in black and observable domain in gray (a), and obtained result for $N = 3$ trial balls (b).

ball. In addition, we introduce the relative error function $\delta_\alpha = |\alpha^* - \alpha^\star|/\alpha^\star \times 100$ in [%], where $\alpha^\star$ is the size (volume) of the true anomaly whereas α^* is the size of the trial ball. The values of these quantities are reported in Table 3, showing that when the center of the target anomaly does not belong to the set of admissible locations X, namely $\xi^\star \notin X$, the algorithm returns a location ξ^* which is the closest to $\xi^\star$. In addition, as expected, the found size α^* converges toward to the true one $\alpha^\star$ when $\mathrm{card}(X)$ increases.

TABLE 3. Example 4: Convergence of the distance function μ_ξ and relative error function δ_α in [%] with respect to the set of admissible locations X.

$\mathrm{card}(X)$	21	113	481	1985
μ_ξ	0.066	0.022	0.022	0.000
δ_α	3.204	1.506	1.544	0.134

7. Concluding remarks

This paper is concerned with an inverse source problem related to the Poisson equation into two spatial dimensions. We have tackled the geometric reconstruction of source locations from internal partial measurements of the potential field. This work is motivated by various engineering applications, such as the gravimetry problem which deals with the identification of the Earth's mass density distribution from measurements of the gravitational field of the surface. The considered inverse problem is reformulated as a self-regularized topology optimization one. The unknown support of the mass distribution is

characterized as the solution to an optimization problem minimizing a given *least-square* functional.

The existence, uniqueness and stability of the optimization problem solution have been established. The second-order topological derivative has been exploited for devising a non-iterative reconstruction algorithm, which is free of initial guess, in the sense that $\omega = \varnothing$, and very robust with respect to noisy data. Our proposed approach is general and can be adapted for solving various inverse problems. In particular, the first order topological derivative gives qualitative information about the hidden anomalies and induces iterative algorithms to reconstruct them. In contrast, the second order topological derivative induces non-iterative reconstruction algorithms given quantitative information on the location and size (volume) of the hidden anomalies. These features are crucial for solving a class of inverse imaging problems in which the stability is the main issue. As supported by the numerical experiments, the resulting second order algorithm is in fact very resilient with respect to noisy data. The main drawback of our approach is the computational cost when $M \approx 2N$ and N increases, remembering that M is the number of admissible locations and N is the number of trial balls. However, it can be combined with well-established and more computationally sophisticated iterative methods [10, 13, 29, 33, 45].

On the other hand, several mathematical issues of high interest have not been discussed in the paper. The identifiability problem is one of them. The full identifiability issue is, however, up to our knowledge, still an open problem which deserves further investigation.

References

[1] A. B. Abda, M. Hassine, M. Jaoua, and M. Masmoudi. Topological sensitivity analysis for the location of small cavities in stokes flow. *SIAM Journal on Control and Optimization*, 48:2871–2900, 2009.

[2] G. Allaire, F. Jouve, and N. Van Goethem. Damage and fracture evolution in brittle materials by shape optimization methods. *Journal of Computational Physics*, 230(12):5010–5044, 2011.

[3] H. Ammari, H. Kang, H. Lee, and J. Lim. Boundary perturbations due to the presence of small linear cracks in an elastic body. *Journal of Elasticity*, 113:75–91, 2013.

[4] S. Amstutz, I. Horchani, and M. Masmoudi. Crack detection by the topological gradient method. *Control and Cybernetics*, 34(1):81–101, 2005.

[5] S. Amstutz and A. A. Novotny. Topological optimization of structures subject to von Mises stress constraints. *Structural and Multidisciplinary Optimization*, 41(3):407–420, 2010.

[6] Yu E Anikonov, BA Bubnov, and GN Erokhin. *Inverse and ill-posed sources problems*, volume 9. Walter de Gruyter, 2013.

[7] H. Attouch, G. Buttazzo, and G. Michaille. *Variational analysis in Sobolev and BV spaces: applications to PDEs and optimization*. SIAM, New York and London, 2014.

[8] D. Auroux, M. Masmoudi, and L. Belaid. Image restoration and classification by topological asymptotic expansion. In *Variational formulations in mechanics: theory and applications*, Barcelona, Spain, 2007.

[9] D Azé. H. Attouch, G. Buttazzo, and G. Michaille. Variational analysis in Sobolev and BV spaces, in MPS–SIAM series on optimization: SIAM and MPS, Philadelphia, 2006. ISBN: 0-89871-600-4 (pbk). *Foundations of Computational Mathematics*, 9(4):515–516, 2009.

[10] J. Baumeister and A. Leitão. *Topics in inverse problems*. IMPA Mathematical Publications, Rio de Janeiro, 2005.

[11] L. J. Belaid, M. Jaoua, M. Masmoudi, and L. Siala. Application of the topological gradient to image restoration and edge detection. *Engineering Analysis with Boundary Element*, 32(11):891–899, 2008.

[12] M. Bonnet. Topological sensitivity for 3D elastodynamic and acoustic inverse scattering in the time domain. *Computer Methods in Applied Mechanics and Engineering*, 195(37-40):5239–5254, 2006.

[13] M. Burger. A level set method for inverse problems. *Inverse Problems*, 17:1327–1356, 2001.

[14] A. Canelas, A. Laurain, and A. A. Novotny. A new reconstruction method for the inverse potential problem. *Journal of Computational Physics*, 268:417–431, 2014.

[15] A. Canelas, A. Laurain, and A. A. Novotny. A new reconstruction method for the inverse source problem from partial boundary measurements. *Inverse Problems*, 31(7):075009, 2015.

[16] A. Canelas, A. A. Novotny, and J. R. Roche. A new method for inverse electromagnetic casting problems based on the topological derivative. *Journal of Computational Physics*, 230:3570–3588, 2011.

[17] F. Caubet, C. Conca, and M. Godoy. On the detection of several obstacles in 2D Stokes flow: Topological sensitivity and combination with shape derivatives. *Inverse Problems and Imaging*, 10(2):327–367, 2016.

[18] F. Caubet and M. Dambrine. Localization of small obstacles in stokes flow. *Inverse Problems*, 28(10):1–31, 2012.

[19] A. Chambolle, V. Caselles, D. Cremers, M. Novaga, and T. Pock. An introduction to total variation for image analysis. In *Theoretical foundations and numerical methods for sparse recovery*, pages 263–340. Gruyter, 2010.

[20] M. C. Delfour and J. P. Zolésio. *Shapes and Geometries. Advances in Design and Control*. Society for Industrial and Applied Mathematics (SIAM), Philadelphia, PA, 2001.

[21] A. El Badia and T. Ha-Duong. An inverse source problem in potential analysis. *Inverse Problems*, 16(3):651–663, 2000.

[22] H.A. Eschenauer, V.V. Kobelev, and A. Schumacher. Bubble method for topology and shape optmization of structures. *Structural Optimization*, 8(1):42–51, 1994.

[23] L. Fernandez, A. A. Novotny, and R. Prakash. Noniterative reconstruction method for an inverse potential problem modeled by a modified Helmholtz equation. *Numerical Functional Analysis and Optimization*, 39(9):937–966, 2018. DOI: 10.1080/01630563.2018.1432645.

[24] L. Fernandez, A. A. Novotny, and R. Prakash. Topological asymptotic analysis of an optimal control problem modeled by a coupled system. *Asymptotic Analysis*, 109(1–2):1–26, 2018. DOI: 10.3233/ASY-181465.

[25] A.D. Ferreira and A. A. Novotny. A new non-iterative reconstruction method for the electrical impedance tomography problem. *Inverse Problems*, 33(3):035005, 2017.

[26] S. Garreau, Ph. Guillaume, and M. Masmoudi. The topological asymptotic for PDE systems: the elasticity case. *SIAM Journal on Control and Optimization*, 39(6):1756–1778, 2001.

[27] Martin Hanke and William Rundell. On rational approximation methods for inverse source problems. *Inverse Probl. Imaging*, 5(1):185–202, 2011.

[28] Frank Hettlich and William Rundell. Iterative methods for the reconstruction of an inverse potential problem. *Inverse problems*, 12(3):251, 1996.

[29] M. Hintermüller and A. Laurain. Electrical impedance tomography: from topology to shape. *Control and Cybernetics*, 37(4):913–933, 2008.

[30] M. Hintermüller and A. Laurain. Multiphase image segmentation and modulation recovery based on shape and topological sensitivity. *Journal of Mathematical Imaging and Vision*, 35:1–22, 2009.

[31] V. Isakov. *Inverse source problems*. American Mathematical Society, Providence, Rhode Island, 1990.

[32] V. Isakov. *Inverse problems for partial differential equations*. Applied Mathematical Sciences vol. 127. Springer, New York, 2006.

[33] V. Isakov, S. Leung, and J. Qian. A fast local level set method for inverse gravimetry. *Communications in Computational Physics*, 10(4):1044–1070, 2011.

[34] Ji-Chuan Liu. An inverse source problem of the poisson equation with cauchy data. *Electronic Journal of Differential Equations*, 2017(119):1–19, 2017.

[35] N.F.M. Martins. An iterative shape reconstruction of source functions in a potential problem using the mfs. *Inverse Problems in Science and Engineering*, 20(8):1175–1193, 2012.

[36] R. Mattoso and A.A. Novotny. Pointwise antennas design in hyperthermia therapy. *Applied Mathematical Modelling*, 89:89–104, 2021.

[37] P. Menoret, M. Hrizi, and A.A. Novotny. On the Kohn–Vogelius formulation for solving an inverse source problem. *Inverse Problems in Science and Engineering*, 29(1):56–72, 2021.

[38] A. A. Novotny and J. Sokołowski. *Topological derivatives in shape optimization*. Interaction of Mechanics and Mathematics. Springer-Verlag, Berlin, Heidelberg, 2013.

[39] A. A. Novotny and J. Sokołowski. *An introduction to the topological derivative method*. Springer Briefs in Mathematics. Springer Nature Switzerland, 2020.

[40] A. A. Novotny, J. Sokołowski, and A. Żochowski. *Applications of the topological derivative method*. Studies in Systems, Decision and Control. Springer Nature Switzerland, 2019.

[41] S. S. Rocha and A. A. Novotny. Obstacles reconstruction from partial boundary measurements based on the topological derivative concept. *Structural and Multidisciplinary Optimization*, 55(6):2131–2141, 2017.
[42] B. Samet, S. Amstutz, and M. Masmoudi. The topological asymptotic for the Helmholtz equation. *SIAM Journal on Control and Optimization*, 42(5):1523–1544, 2003.
[43] A. Schumacher. *Topologieoptimierung von bauteilstrukturen unter verwendung von lochpositionierungkriterien*. Ph.D. Thesis, Universität-Gesamthochschule-Siegen, Siegen - Germany, 1995.
[44] J. Sokołowski and A. Żochowski. On the topological derivative in shape optimization. *SIAM Journal on Control and Optimization*, 37(4):1251–1272, 1999.
[45] P. Tricarico. Global gravity inversion of bodies with arbitrary shape. *Geophysical Journal International*, 195(1):260–275, 2013.
[46] N. Van Goethem and A. A. Novotny. Crack nucleation sensitivity analysis. *Mathematical Methods in the Applied Sciences*, 33(16):1978–1994, 2010.
[47] M. Xavier, E. A. Fancello, J. M. C. Farias, N. Van Goethem, and A. A. Novotny. Topological derivative-based fracture modelling in brittle materials: A phenomenological approach. *Engineering Fracture Mechanics*, 179:13–27, 2017.

(M. Hrizi) Monastir University, Department of Mathematics, Faculty of Sciences Avenue de l'Environnement 5000, Monastir, Tunisia
Email address: mourad-hrizi@hotmail.fr

(A.A. Novotny) Laboratório Nacional de Computação Científica LNCC/MCT, Coordenação de Métodos Matemáticos e Computacionais, Av. Getúlio Vargas 333, 25651-075 Petrópolis - RJ, Brasil
Email address: novotny@lncc.br

(M. Hassine) Monastir University, Department of Mathematics, Faculty of Sciences Avenue de l'Environnement 5000, Monastir, Tunisia
Email address: maatoug.hassine@enit.rnu.tn